TOPICAL REVIEW • OPEN ACCESS

Recent advances in petahertz electric field sampling

To cite this article: A Herbst *et al* 2022 *J. Phys. B: At. Mol. Opt. Phys.* **55** 172001

View the article online for updates and enhancements.

You may also like

- Dipoles in blackbody radiation: momentum fluctuations, decoherence, and drag force
  Kanu Sinha and Peter W Milonni

- *Ab initio* calculations of the hyperfine structure of ^{109}Cd, $^{109}Cd^+$ and reevaluation of the nuclear quadrupole moment $Q(^{109}Cd)$
  Benquan Lu, , Xiaotong Lu et al.

- Modeling the behavior of two-electron atom at critical nuclear charge
  Ruo Yu Zheng, Li Guang Jiao, Aihua Liu et al.

Topical Review

Recent advances in petahertz electric field sampling

A Herbst[1,2], K Scheffter[1,2], M M Bidhendi[1,2,3], M Kieker[1,2,4],
A Srivastava[1,2] and H Fattahi[1,2,∗]

[1] Max Planck Institute for the Science of Light, Staudtstr. 2, 91058 Erlangen, Germany
[2] Department of Physics, Friedrich-Alexander University Erlangen-Nürnberg, Staudtstr. 7, 91058
Erlangen, Germany

E-mail: hanieh.fattahi@mpl.mpg.de

CrossMark

Abstract

The ability to resolve the complete electric field of laser pulses from terahertz to mid-infrared
spectral ranges has enriched time-domain spectroscopy for decades. Field-resolved
measurements in this range have been performed routinely in ambient air by various
techniques like electro-optic sampling, photoconductive switching, field-induced second
harmonic generation, and time stretch photonics. On the contrary, resolving the electric field of
light at the near-infrared spectral range has been limited to attosecond streaking and other
techniques that require operation in vacuum. Recent advances are circumventing these
shortcomings and extending the direct, ambient air field detection of light to petahertz
frequencies. In the first part of this letter, recent field-resolved techniques are reviewed. In the
second part, different approaches for temporal scanning are discussed, as the temporal
resolution of the time-domain methods is prone to temporal jitter. The review concludes by
discussing technological obstacles and emerging applications of such advancements.

Keywords: field-resolved metrology, petahertz electric field sampling, ultrashort pulses

(Some figures may appear in colour only in the online journal)

1. Introduction

Laser has been a fundamental tool to simultaneously excite
and interrogate dynamics in matter. In combination with the
advances in the generation of laser pulses with ever shorter
temporal duration, this unique property has allowed for mon-
itoring ever faster dynamics. In fact, the first observation of
molecular dynamics and the birth of femtochemistry [1] was
empowered by the availability of multi-cycle femtosecond
pulses [2–7].

When the temporal duration of a short pulse reaches the
few-cycle regime, the relative phase offset between the enve-
lope of the pulse and the fast oscillating electric field at car-
rier frequency becomes evident and crucial. Evaluation of
the carrier-envelope phase (CEP) offset via f−2f interferom-
etry [8, 9] has enabled the precise control of the oscillat-
ing electric field under the envelope of a short pulse [10]
and the emergence of the entirely new research field of fre-
quency comb metrology [11–13]. In 2001, the first isolated
attosecond pulses were generated from the interaction of

CEP-stable, nearly single-cycle pulses and a noble gas, paving the path towards a better understanding of the ultrafast motion of electrons [14].

Limited by the bandwidth of the available technology for compensating the spectral phase of super-octave high energy pulses [15–20], shorter pulses and even light transients were generated by coherent field synthesis [21–27]. Here, by constructive interference of several few-cycle pulses at different carrier frequencies, temporally confined waveforms with a temporal duration shorter than individual pulses are generated. Furthermore, the waveforms can be shaped arbitrarily by fine-tuning the relative phase and amplitude between the superimposed pulses.

The electric field of ultrashort pulses upon interaction with media contains a detailed description of the internal dynamics of the atoms, molecules, or solids that it encountered. Resolving the electric field of light with sub-cycle resolution after it interacts with the sample under scrutiny allows obtaining precise time-frequency analyses of the system's dynamics. In particular, light transients offer an unprecedented degree of control over atomic-scale electronic motions and can induce dramatically different responses in the electronic system of matter [28–32].

But how can one measure and characterize such short pulses in the time domain? 'Isn't it that to measure a short event in time, you must use a shorter one?' [33]. Over the last decades, dozens of different techniques have been developed to characterize few-cycle pulses, which can be divided into two major categories: (i) techniques, which rely on the determination of the spectral amplitude and phase of the electric field [34–60], which have been even used for CEP stabilization [35, 61, 62], (ii) techniques for the direct measurement of the electric field of ultrashort pulses in the time domain, offering high temporal resolution [63–72].

Field detection methods like electro-optic sampling (EOS) [73], photonic time stretch [74], and photoconductive switching [75] at terahertz (THz) and mid-infrared (MIR) spectral ranges offer high sensitivity and dynamic range at sub-cycle resolution. They have opened several new avenues in fundamental investigations like sub-cycle resolution quantum electrodynamics and quantum optics [76–80], the tracing of electron wavepackets [81], Bloch oscillations dynamics [82], sensitive molecular fingerprinting in biological samples [70], and other nonlinear phenomena [83–85].

A fast temporal gate (ideally with a duration below the half-cycle duration of the field oscillation to be measured) is the primary requirement for extending the detection bandwidth of field-resolved measurements to petahertz (PHz) frequencies. In 2001, the generation of isolated attosecond pulses via high harmonic generation (HHG) [86, 87] provided such short gate pulses and allowed for the direct measurement of the electric field at near-infrared (NIR) frequency ranges by attosecond streaking [31, 88, 89].

In a streak camera, upon the interaction of the attosecond pulses with the atoms of a noble gas, the ionised gas atoms emit free photo electrons. Simultaneously applying the sample field to the atoms accelerates the free electrons and shift their final momentum in proportion to the vector potential of the sample

field at the instant of ionization. Therefore, the electric field of the sample pulse can be mapped by changing the temporal delay between the two fields, and recording the electron's momentum at a time-of-flight spectrometer. Alternatively, sub-cycle electron trajectories during the HHG process can be used to measure a light wave [90–92]. While powerful, these techniques require significant pulse energies for the HHG process, a costly time-of-flight spectrometer, as well as an expensive and complex high-vacuum setup in order to avoid the absorption of extreme ultraviolet (UV) pulses in ambient air. These technical challenges have limited their application and slowed down their practicality.

Over the past few years, various innovative solutions have been demonstrated, and remarkable progress has been made in developing alternative field-sensitive methods operating in ambient air. Like attosecond streaking, the majority of these field-sampling techniques rely on the use of a short auxiliary pulse providing a sub-cycle nonlinear gate, or on a strong-field response of matter, such as tunnel ionization, high-order harmonic generation or multi-photon excitation in solids.

Figure 1 summarizes the common pulse characterisation techniques at optical frequencies and compares their performance in terms of sensitivity and frequency coverage. The offered detection sensitivity and bandwidth in field sampling techniques, in addition to their ambient air operation, pave the path not only for sub-cycle electron-dynamic interrogation of matter, but also for novel spectro-microscopic techniques with an unprecedented spatial and temporal resolution.

This review presents a summary of the growing field of field-resolved metrology at optical frequencies with an outlook on its emerging applications. In all the techniques described below, short laser pulses in combination with different nonlinear phenomena are used to probe the electric field of an arbitrary pulse. Throughout the paper we labeled the pulse/event which enables temporal gating the 'gate pulse/event' and the one that is being measured the 'sample pulse'.

2. Field sampling based on strong-field electron dynamics

In strong-field approximation for an atomic system [93], the strong-field interaction of light and matter can be described by the Keldysh parameter γ [94]:

$$\gamma = \omega \frac{\sqrt{2mI_0}}{eF},\tag{1}$$

where ω is the carrier frequency of the strong field, F is the peak field strength, I_0 is the ionization potential of the gas medium, and e and m are the electron charge and effective electron mass, respectively. In solids, the strong-field approximation translates into the neglect of excitonic effects. The Keldysh parameter becomes:

$$\gamma = \omega \frac{\sqrt{mE_g}}{eF},\tag{2}$$

where E_g is the transition bandgap. The presence of a strong electric field in a dielectric medium injects electrons from the
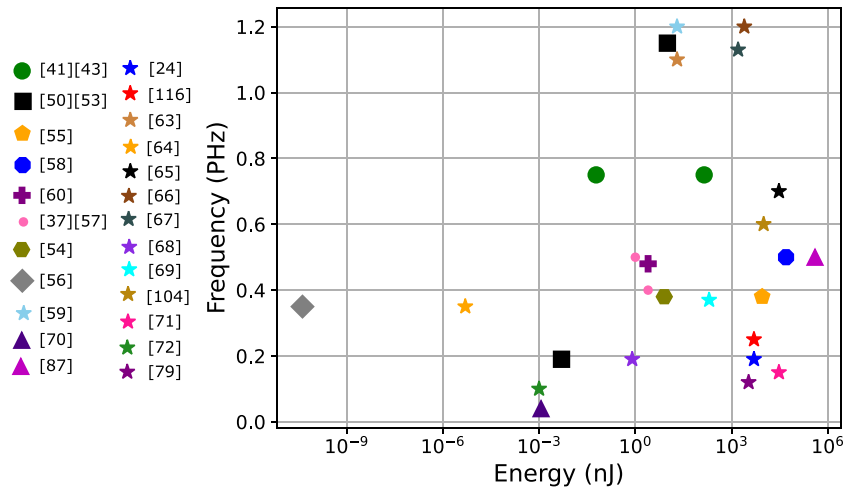
Figure 1. Detection bandwidth and sensitivity of various pulse characterization methods at optical frequencies and below. Each shape represent a characterization technique. Data points related to the field measurement techniques operating in ambient air are represented by stars, while triangles demonstrates the field-resolved methods operating in vacuum. The other symbols show the techniques characterizing the complex envelope of a laser pulse. Estimated energy-value in [68].

valence band into the conduction band. The Keldysh parameter classifies adiabatic tunneling for $\gamma \ll 1$, and frequency-dependent multiphoton excitation for $\gamma \gg 1$ [95–103]. Since for both, multi-photon absorption and tunneling ionization, high field strengths are required, the type of the transition is mainly dominated by the frequency of the incident wave.

Upon the interaction of an intense laser field with atoms, molecules, and solids at the tunneling regime, electron dynamics directly follow the electric field of the laser pulses, with exponential dependence. Therefore, they are temporally confined to subcycle timescales, making them suitable for serving as a fast gate for electric field sampling.

2.1. Photoconductive sampling in gas

In 2018, Park *et al* demonstrated how the tunneling ionization in a gas could generate an ultrashort gate event for resolving the electric field of an arbitrary sample pulse up to 1.5 PHz, limited by the absorption in the lightest gases of H and He [104]. The technique is based on tunneling ionization with a perturbation for the time-domain observation of an electric field (TIPTOE). Upon the interaction of an intense, sub-cycle laser pulse with a gas, the atomic potential is deformed. At each half-cycle of the laser pulses, part of the wave-function tunnels through the Coulomb barrier creating an electron wave packet, which is used as the fast temporal gate to probe the electric field of a sample pulse (E_S).

Due to the exponential dependence of the ionization rate at the peak of the pulse, the fast temporal gate can be temporally confined to 190 as [104]. When the weak arbitrary sample pulse is superimposed with the intense laser pulse at the same polarization direction, it gently perturbs the process of the tunneling ionization and consequently the total ionization yield by δN. For intense pulses as short as 1.5 optical cycles, the ionization event effectively occurs only at the peak of the electric field. Therefore, the modulation of the ionization yield becomes proportional to the field amplitude of the weak sample pulse:

$$\delta N(\tau) \propto E_S(\tau) \qquad (3)$$

that can be measured directly as an electric current (see figure 2). Employing this technique, direct sampling of the electric field up to 0.6 PHz in ambient air [104] and over a wide spectral range spanning from UV to MIR [67] by collecting the ion current or the plasma fluorescence intensity [105] as a function of the time delay between the two pulses has been demonstrated.

As TIPTOE relies on field ionization, it is an utterly phase-matching-free technique. Moreover, the method can resolve the electric field of multi-cycle laser pulses as long as the duration of the intense laser pulse is three times shorter than the transform-limited duration of the weak sample pulse [104]. However, TIPTOE requires intense nearly single-cycle pulses to generate a temporally confined gate. The two interacting pulses have to be CEP-stable, and the precision of the measurement is prone to their relative temporal jitter. Furthermore, the ionization yield can also be modulated by the power fluctuation of the laser pulses unless differential detection is employed.

Alternatively, photo-emitted electrons, which are generated via the interaction of a strong field and air, can be used to probe the electric field of an arbitrary sample pulse, similar to attosecond streaking [65, 71]. Superposition of the strong field with a weak sample field induces an asymmetry in the angle-resolved photo-emission of electrons. The induced current is measured by positioning two electrodes in the asymmetry plane.

Here the strong laser field has to be polarized along the direction of the electrodes to avoid any background signal. The weak waveform is polarized across the electrodes. It displaces the electrons toward one of the electrodes and separates them from positively charged ions. The separation leads to the formation of a dipole, which is screened by
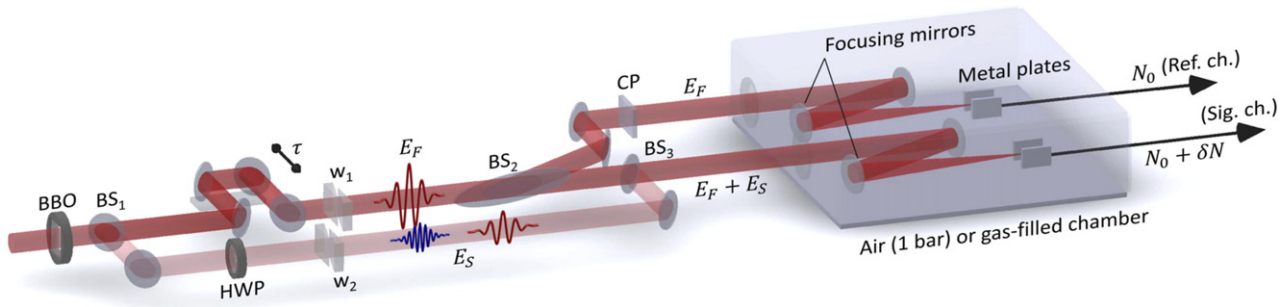
J. Phys. B: At. Mol. Opt. Phys. **55** (2022) 172001

Topical Review

Figure 2. Weak sample pulses (E_S) are generated via second harmonic generation. The residual fundamental laser pulses (E_F) after second harmonic generation serve as the intense excitation pulse for field-sampling. A portion of the intense pulse is superposed with the sample pulse in air for direct electric field detection, where the ionization yield $N_0 + \delta N$ is measured. The other portion is used as a reference arm for differential detection, where the ionization yield N_0 of the intense pulse is measured. BS: beam splitter; w: wedges; HWP: half wave plate; CP: compensation plate [104].

the metal electrodes and results in a measurable current (see figure 3). The electric field of the weak pulse is retrieved by recording the measured current at a different relative time delay of the two laser fields. Field sampling in air for frequencies up to 0.13 PHz was reported by employing this technique [71].

The induced asymmetry in angle-resolved photoemission can be caused by the combined action of the laser fields and the Coulomb potential of the ion on the electron. In the absence of the sample field, this asymmetry is parallel to the injection (gate) field (figure 3(b)), while the symmetry with respect to the field direction of the electrodes is broken by the driving field (figure 3(c)) [65]. The electrons undergo ponderomotive motion in the strong field direction, while they are being accelerated by the weak waveform, leading to a complicated Coulomb-laser-coupling. Similar to attosecond streaking, this coupling influences the relative timing of the signal [106–108]. The simulation results in [65] confirm that the measured signal as a function of time delay approximates the vector potential of the weak waveform, but with a significant delay. Similar to TIPTOE, this technique requires ultrashort, CEP-stable laser pulses with high field strength to probe the electric field of a weak pulse and is sensitive to the relative timing jitter of the two pulses.

2.2. Photoconductive sampling in solid

A strong laser field can induce rapid changes to the electronic properties of dielectric solids by transforming the dielectric into a state of highly increased polarizability [98]. The light-field-induced currents upon this interaction results in a macroscopic charge separation that is detectable in an external circuit. Due to the high nonlinearity of the carrier injection process in wide bandgap materials, mostly the optical cycles with high electric field strength contribute to this interaction. Therefore, the gate event is temporally well confined and effectively shorter than the driving pulse.

This temporary modification of dielectrics forms the basis of the field sampling method called nonlinear photoconductive sampling [63]. Here, a strong single-cycle gate pulse with 1 to 2 V $Å^{-1}$ field strength interacts with crystalline quartz, which induces a transition from the filled valence to the empty

conduction band. This transition probability is temporally confined to sub-fs duration and strongly localized to instants slightly after the peak of the electric field.

At the temporal overlap of the cross-polarized weak sample pulse and the intense laser field, the injected electron–holes are displaced in the band structure and form a macroscopic dipole. The induced dipole gives rise to a screening signal and thus a measurable current in the pair of electrodes. Scanning the relative delay between the two fields allows for the complete field characterization of the weak sample pulse from MIR to UV (figure 4). The rate of energy deposition in this scheme is approximately proportional to the eighth power of the electric field. Therefore, carrier injection is temporally confined to a sub-500 as time interval. The authors demonstrate up to 1 PHz sampling bandwidth at a detection dynamic range of 30 dB. Like gas-based techniques, CEP-stable, single-cycle pulses and temporal synchronization of the interacting pulses are prerequisites for resolving the electric field of arbitrary waveforms.

In an alternative study, a field-sampling technique based on the sub-cycle changes in the reflectivity of dielectrics, when subjected to a strong field was demonstrated [66]. A strong, few-cycle pulse with a field strength of 0.78 to 1.33 V $Å^{-1}$ excites electron dynamics in a quartz crystal. In the reciprocal space and at the minimum bandgap (zone center), due to the coherent multiphoton excitation, the electrons can transit from the valence band to the conduction band at the peak of the electric field and are accelerated towards the Brillouin zone boundaries, following the vector potential of the driver field in the conduction band. As the sign of the electric field in the subsequent half-cycle changes, the electrons accelerate back to the other side of the Brillouin zone boundary crossing the zone center [109]. At the zone center, there is a possibility for population transfer from the conduction band back to the valence band, which results in a sub-cycle modulation of the refractive index. Hui *et al* demonstrate that probing the sub-cycle modulation of the reflectivity allows for the full reconstruction of the electric field of the strong pulse.

The probe pulse can be generated by using a mask to split the main pulse into two beams: intense sample pulses to induce the dynamic and weak pulses to probe the induced sub-cycle
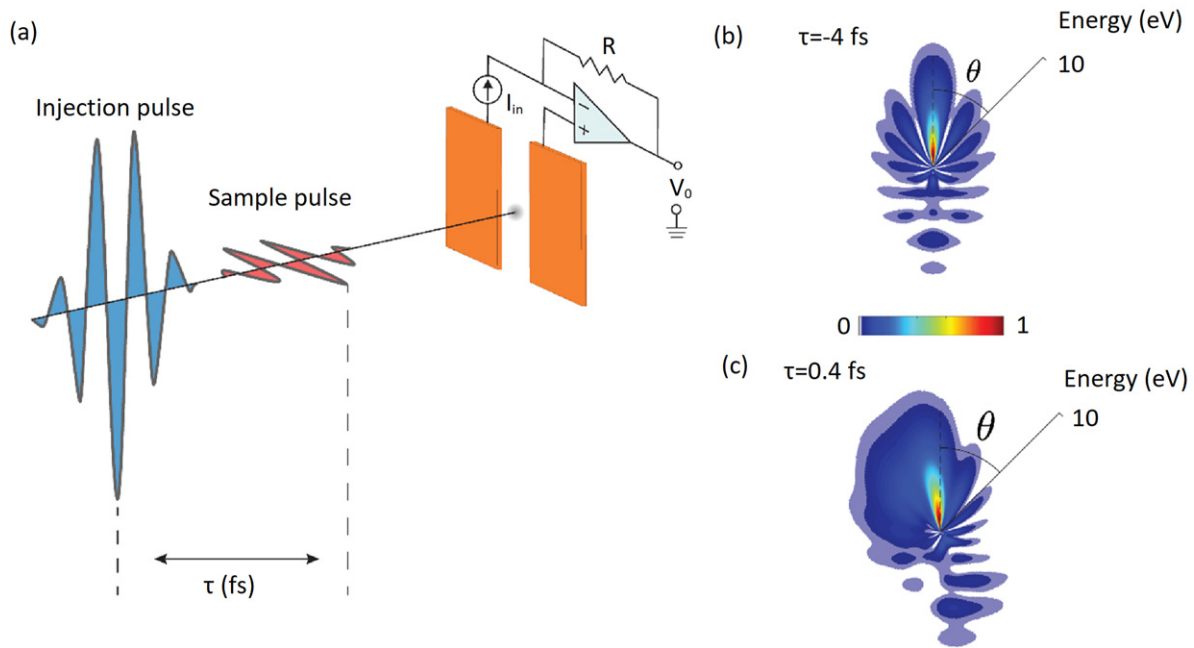
Figure 3. (a) An intense optical pulse with vertical polarization generates free carriers in the gas between the electrodes. Simultaneously, collinear superposition of a weaker sample pulse with an orthogonal polarization induces an angular asymmetry in the photo-emission of electrons, causing an imbalance along the direction of the electrodes. The electrodes screen the resulting dipole, inducing a detectable current in the measurement circuit. (b) and (c) The simulated unperturbed and perturbed angle-resolved energy distributions of the free electrons released by a vertically polarized, 15 GV m^{-1}, 2.2 fs pulse in hydrogen [65] (notation adapted).
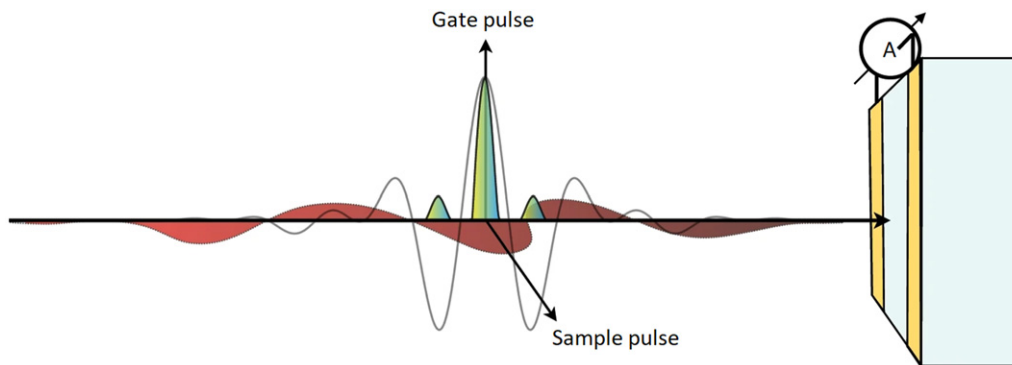

Figure 4. Upon the interaction of a nearly single-cycle strong gate pulse and a quartz crystal, a transition from the valence to the conduction band in the material is induced. This transition is temporally restricted to field crests. In the presence of the orthogonally polarized weaker sample field, the light-field-induced currents result in a detectable macroscopic current between the gold electrodes [63].

reflectivity changes. The two beams are focused on a 100 μm-thick quartz crystal. An optical spectrometer is used to measure the reflected spectrum of the probe beam from the sample at various delays (figure 5). The technique offers a broad detection bandwidth and is not restricted by phase mismatch. However, the detection sensitivity is restricted to the pulses with high-field strength.

In 2021, Liu *et al* reported on the first field-sampling technique based on electron tunneling in solids [69]. In a setup similar to TIPTOE, the solid-state TIPTOE technique employs tunneling or multiphoton excitation as a fast gate process. In the tunneling regime, an intense pulse with central frequency well below the bandgap excites the valence band electrons into the conduction band of a dielectric. The excitation fraction is

perturbed by a weak sample pulse and its relative changes can be detected by monitoring the visible band fluorescence emission from the crystal surface on sub-nanosecond time scales (figure 6) [110, 111]. The authors demonstrate full characterisation of an electric field with spectral components spanning from 2.9 μm to 4 μm and a few-cycle pulse centered at 1.1 μm.

3. Field sampling based on short optical gate pulses

Short optical probe pulses have been used to sample the electric field of waveforms from THz to MIR and recently to visible spectral range by EOS [24, 59, 73, 112–119].
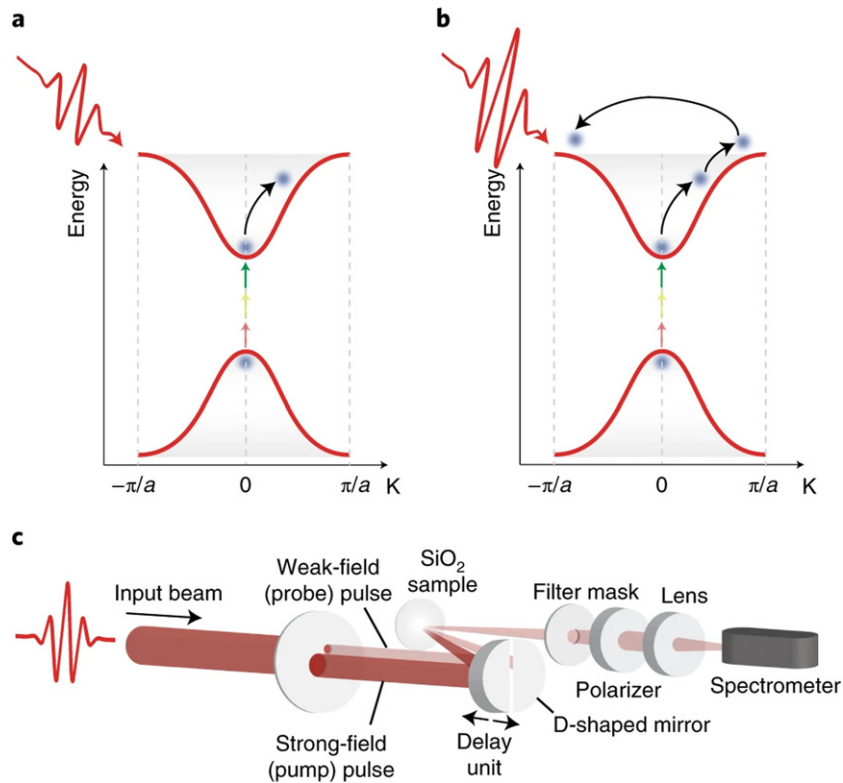
Figure 5. (a) and (b) The interaction of a laser field and a dielectric solid at critical field strengths results in its sub-cycle refractive index modulation due to multiphoton carrier excitation from the valance band to the conduction band, aswell as electron motion dynamics in the conduction band (shown in reciprocal space). (c) Experimental setup of the all-optical implementation. A spatial mask is used to split the main beam to two parts of different intensities: a strong pump to drive the strong field dynamics and a weaker probe to detect the resulting changes in refractive index. Subsequently the two beams are focused on a 100 μm thick SiO_2 crystal. A piezo-stage controls the relative delay between the two pulses. A spectrometer measures the reflectivity of the weak pulse at each delay point, while a polarizer and a one-hole mask enhance the signal-to-noise ratio of the reflectivity modulation measurements [66].

In EOS, gate pulses and sample pulses propagate collinearly in a nonlinear crystal. When the phasematching condition is fulfilled, new spectral components at the sum and difference frequencies of the two interacting pulses are generated, which have partial spectral overlap with the gate pulse [118, 119]. The field-sensitive signal arises from the interference between the original gate photons and the newly generated photons, containing phase information similar to homodyne detection. Spectral short and long pass filters in this setup isolate the spectral region of the gate pulse that has overlap either with the sum or difference frequency signal [122].

In the absence of the sample pulse, an ellipsometer is designed in a way that the gate pulse is equally split on two photo diodes of a balanced detector, and the detected voltage is zero. A nonzero voltage is detected in the presence of the sample pulse, when the polarisation of the gate pulse is modified by interference with the newly generated components. This change in polarisation varies relative to the temporal delay between the gate pulse and the sample pulse (figure 7(a)). This ellipsometric analysis of the interfering fields gives direct access to either the electric field of the sample field or its Hilbert transform [119]. The excess technical noise of the gate pulse is suppressed by a lock-in amplifier and the balanced

detection, leaving the shot noise of the gate pulse the limiting factor on detection sensitivity.

The description of EOS is simplified, when the spectrum of the sample pulse lays within the far-infrared or THz spectral range. Here, the oscillation cycle of the sample pulse is significantly longer than the temporal duration of the gate pulse at NIR. The electric field of the sample pulse can be assumed to be a quasi-static electric field in relation to the gate pulse. This quasi-static field induces a birefringence in the crystal due to the electro optic effect (hence the name 'electro optic sampling'), resulting in a measurable change in polarisation of the gate pulse. This picture can be motivated by the nature of the electro optic effect, or Pockels-effect, as it is described by second order nonlinear mixing of two fields, where one of them is a static electric field. [73, 123].

One way to enhance the detection sensitivity in EOS beyond the limitations imposed by the shot noise of the gate pulses is to use the overlapped region of the difference and sum frequency signals for phase information retrieval. As the complete interference between the sum and difference frequencies is only possible at the center of the gate spectrum, the suppression of the background relies on polarization filtering of the gate pulses (figure 7(b)). Employing this technique allows for the complete retrieval of the sample pulse with high detection sensitivity, but with sign ambiguity [121].
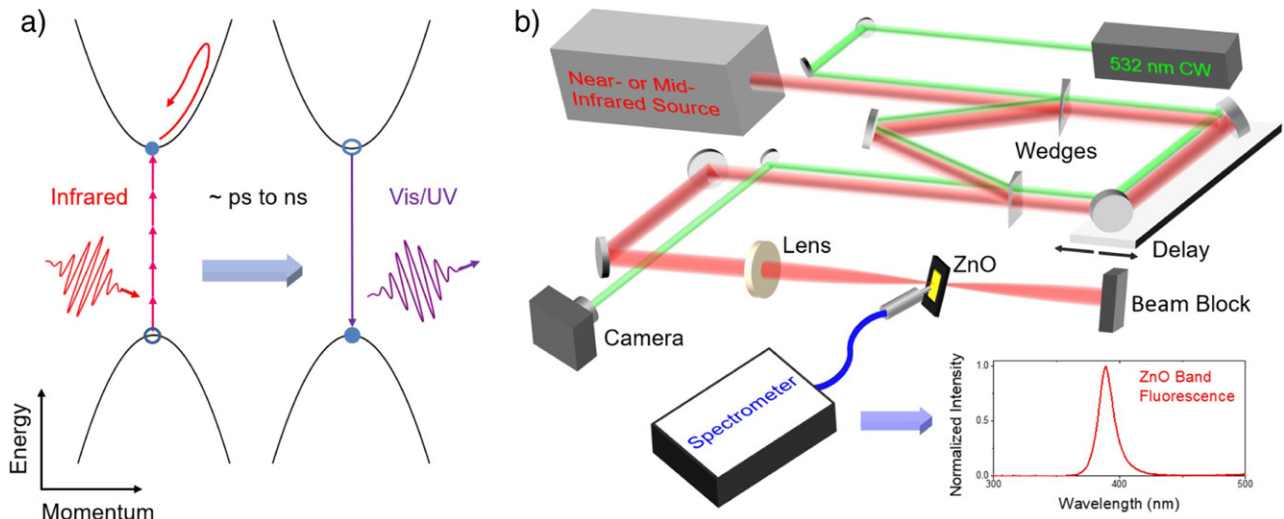
J. Phys. B: At. Mol. Opt. Phys. **55** (2022) 172001

Topical Review

Figure 6. Solid-state TIPTOE is based on multiphoton absorption—shown in (a)—or field-induced tunneling from the valence band to the conduction band of the solid in the presence of an intense electric field. The excitation can be measured in the form of fluorescence, when the excited electrons recombine with the holes in the valence band under emission of a photon. The excitation is temporally confined to the strong gate pulse, also it is perturbed by the presence of a weak sample field. Therefore, it acts as a short gate event for field sampling. (b) Schematic setup of solid-state TIPTOE. The perturbed excitation fraction is monitored by detecting the changes in the fluorescence of ZnO at various delays. Inset: typical band fluorescence spectrum of ZnO [69].
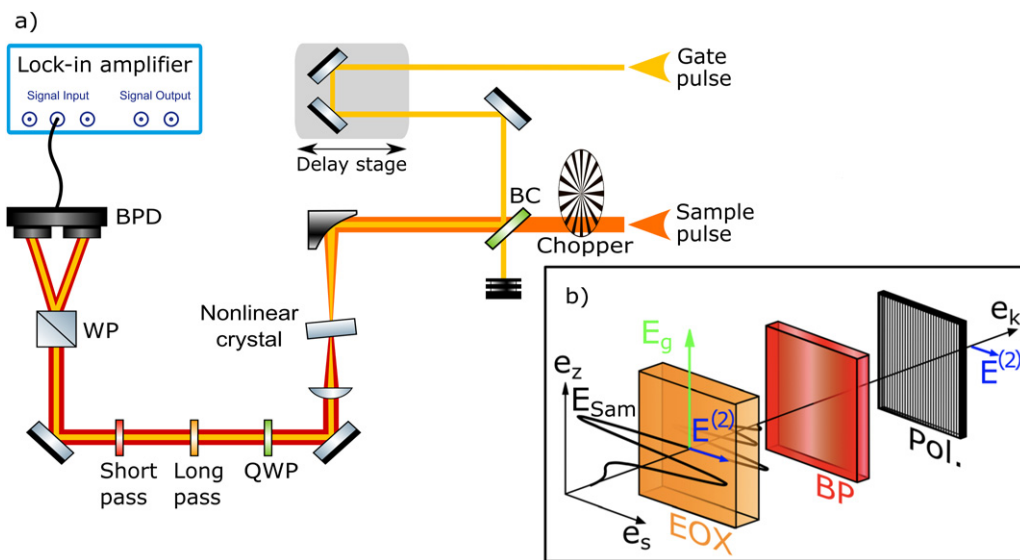

Figure 7. (a) Schematic EOS setup. Sum frequency or difference frequency signal of the gate and sample pulse are generated in a nonlinear crystal. The region with spectral overlap between the newly generated frequencies and the gate pulse are spectrally isolated. An ellipsometer detects the changes in the polarisation state of the gate pulse resulting from the interference with the newly generated frequencies. The sample pulse is periodically blocked to allow lock-in detection BC: beam combiner; QWP: quarter-wave plate; WP: Wollaston prism; BPD: balanced photodetector [120]. (b) The sample pulse E_{Sam}, the gate pulse E_g and the newly generated field $E^{(2)}$. In this alternative detection scheme, the newly generated components are isolated using a band-pass filter (BP) and a polarizer (Pol.). This scheme does not require balanced detection. EOX: electro-optic crystal [121].

EOS offers an appealing detection sensitivity and dynamic range. Nonetheless, its direct extension towards multi-PHz frequencies would require a gate pulse with twice the frequency of the field to be sampled [116]. Generation, handling, and dispersion-free propagation of such pulses is a major challenge. GHOST, generalized heterodyne optical-sampling technique, addresses these deficiencies (see figure 8). In GHOST, the sum or difference frequency generation between the gate

and the sample pulses provides a heterodyne signal, while the higher harmonics of the gate pulse act as a local oscillator. The phase information of the sample pulse is extracted upon the four-wave mixing interaction of the higher harmonics of the gate pulse and the heterodyne signal. The concept shares some similarities with air-biased-coherent-detection at THz range [124, 125]. The detection bandwidth can be scaled to higher frequencies by choosing the higher harmonics of the
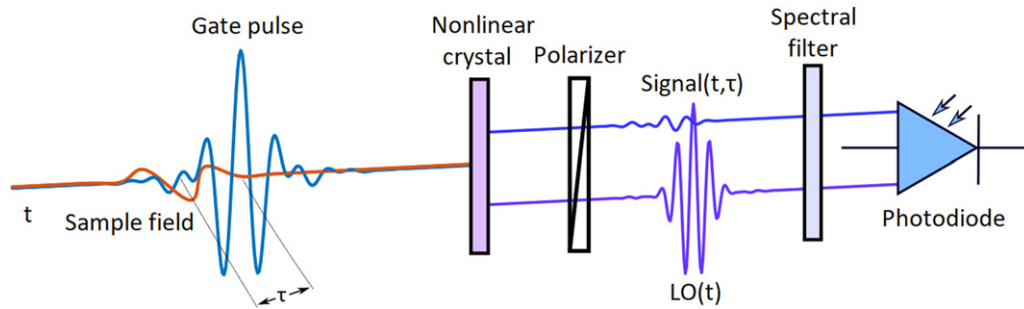
Figure 8. Two pulses overlap in a nonlinear crystal: a sample field and a gate pulse. As a result, two waves are generated: a local oscillator (LO) resulting from nonlinear propagation of the gate pulse in the crystal, and a signal, which is the result of nonlinear mixing of both input pulses. These waves pass through a polarizer and a spectral filter and are detected using a photo diode [59].
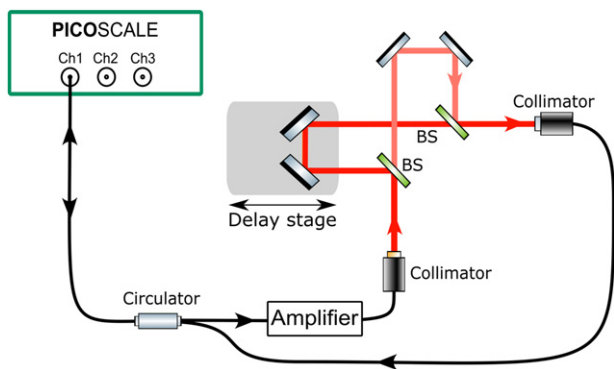

Figure 9. Interferometric delay tracking setup. A three-port fiber circulator separates the incoming laser from the outcoming interference signal. A phase-modulated continuous-wave laser diode is used for interferometric measurement. A Mach–Zehnder interferometer like this can be implemented on top of an optical delay line to track the timing jitter of the pulses [120].
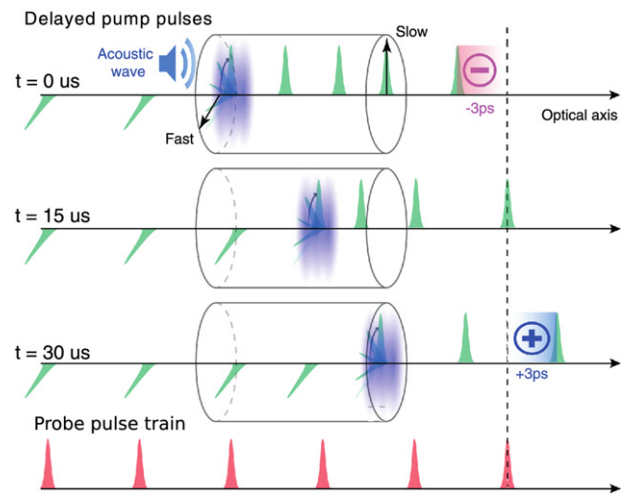

Figure 10. Principle of an acousto-optical delay line. An incident ordinarily polarized pulse diffracts at an acoustic wave into the extraordinary axis [132].

gate pulse. However, the CEP of the retrieved waveform does not follow the CEP changes of the sample waveform. It has been demonstrated that field detection via GHOST supports up to 1.25 PHz detection bandwidth with a signal-to-noise ratio of approximately 30 dB [59].

4. Time scanning methods

All techniques which are described in this paper share a similar concept: the electric field of a sample pulse is resolved by monitoring the variations of a correlation signal, which is generated through a fast event at different temporal delays. Therefore, the measurement's precision depends on the temporal stability and the jitter between the two interacting pulses. The intrinsic synchronization between the two pulses are assured as they originate from the same source. However, additional temporal jitter is introduced by air turbulence, mechanical vibrations of optical components, temperature drifts and the finite stability of the frontend. In what follows, different available techniques for enhancing the temporal stability in field-resolved measurements are reviewed.

4.1. Interferometric delay tracking

Two conventional methods to temporally delay two pulses relative to each other are step-scan or rapid-scan techniques, where the temporal delay between two pulses is varied by moving a retro-reflector mounted on a mechanical delay stage. The position of the stage can be determined either by the linear encoder of the delay stage or by a Michelson-type sensor head for precise tracking of the stage movements [126, 127]. However, in these techniques the recorded position does not represent the actual relative delay between the two pulses at the moment of interaction.

Alternatively interferometric delay tracking can be used to precisely track the relative delay. Here a phase modulated continuous-wave laser is coupled to the optical path of the sample pulse and the gate event from the moment of separation until their recombination. The exact optical path difference of the two arms is extracted from the interference signal via quadrature detection. The layout of a typical interferometric delay tracking setup is shown in figure 9. Employing this technique allowed for delay tracking with 10 as precision [120, 128].
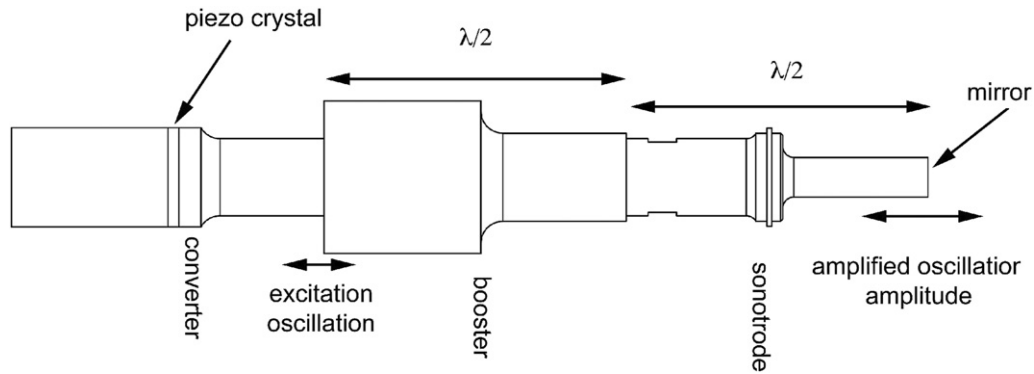
Figure 11. Mechanical resonator for constructing an oscillating mirror. The rapid mechanical resonator consists of a converter, a booster, and a sonotrode. The converter transforms an electric signal into an ultrasonic acoustic signal via the piezo electric effect, resulting in an oscillation at its resonant frequency. The booster alters the oscillation amplitude according to the relative mass ratio at the input and the output. The sonotrode further amplifies the oscillation and transmits it to the reflective element. Here, λ refers to the wavelength of the acoustic wave [134].
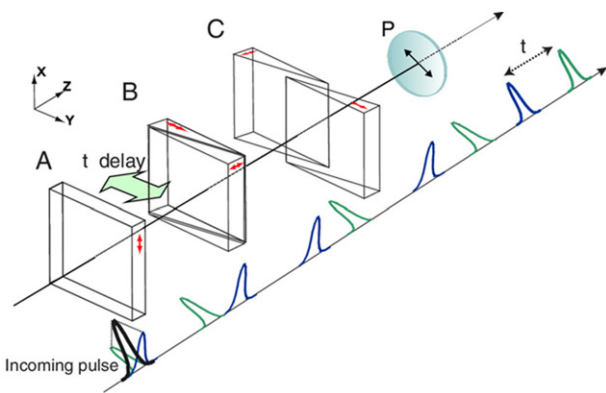

Figure 12. TWINS uses birefringence to generate a tunable time delay between two collinear pulses. First a flat block A introduces a constant negative delay between the two orthogonal polarisation components of the input pulse. Wedge pair B introduces a tunable time delay between the pulses. Wedge pair C corrects the wavefront tilt, the angular dispersion and allows dispersion tuning. This results in two cross polarised output pulses with a time delay t, that are projected on a common axis by a polarizer P [138].

4.2. Acousto-optic modulator delay line

The acousto-optic programmable dispersive filter (AOPDF), also known as Dazzler, consists of a birefringent crystal in which an ordinarily polarized laser pulse propagates collinearly with a polychromatic acoustic shear wave. Upon acousto-optic interaction, the pulse diffracts into the extraordinary axis depending on the applied acoustic signal. Since its first proposal by P Tournois [18], the AOPDF has been used not only for pulse shaping and dispersion control, but also as a rapid scanning delay line [129–133].

The working principle of an acousto-optical delay line is depicted in figure 10. Various temporal delays can be introduced by confining the acoustic wave to a wave packet smaller than the length of the crystal (blue area in figure 10). Since the speed of light inside the bulk medium is six orders of magnitude higher than the velocity of the acoustic wave packet, the position of the acoustic wave packet appears to be stationary for an incoming laser pulse. Between two consecutive laser pulses, the position of the acousto-optic interaction changes as the acoustic wave packet travels a certain distance inside the crystal. Due to the difference in the refractive index of the ordinary (n_o) and extraordinary (n_e) axis, the diffracted pulse propagates with a velocity different from the non-diffracted pulse. Therefore, the time difference between one pulse entering the crystal and the diffracted pulse leaving the crystal depends on the diffraction position. Since the speed of the shear acoustic wave v_{sound} inside the crystal is known, the acoustic wave packet travels a distance $\Delta x = \frac{v_{sound}}{\nu_{rep}}$ between two consecutive optical pulses with repetition rate ν_{rep}. Consequently, the introduced time delay Δt increases with each laser pulse by

$$\Delta t_{n,n+1} = (n_e - n_0)\frac{v_{sound}}{c \cdot \nu_{rep}}. \tag{4}$$

One significant benefit of the acousto-optical delay line is its high stability and repeatability at scan frequencies ranging up to 36 kHz [131]. Since the delay line contains no moving parts, it is not prone to beam-pointing fluctuations. Furthermore, the difference in the time delay between two consecutive pulses (equation (4)) depends solely on material properties and the repetition rate of the laser.

The high stability of the delay line allows for interleaved scanning, where multiple cycles of the acousto-optical delay line are used to create one scan with a shorter step size between the sampled time delays. Here, the launch of the acoustic wave packet is delayed for each cycle by $\frac{1}{k \cdot \nu_{rep}}$ with respect to the previous one, resulting in a factor of k more sample points and a smaller time delay step size. Schubert *et al* reported on a scan with $k = 128$ interleaved cycles at a repetition rate of 40 MHz and a single cycle scan rate of 34 kHz in a TeO₂ crystal. The authors achieved a temporal resolution of 39 as [129].

Since the acousto-optical delay line is in its nature an AOPDF, the acoustic pulse can still act as a dispersive filter for dispersion control or pulse shaping, while scanning the group delay. This has been used to compensate for dispersion [131, 132] as well as for spectral focusing [133]. However, simultaneous phase compensation of few-cycle pulses in the delay line is not practical. Moreover, the bandwidth of the
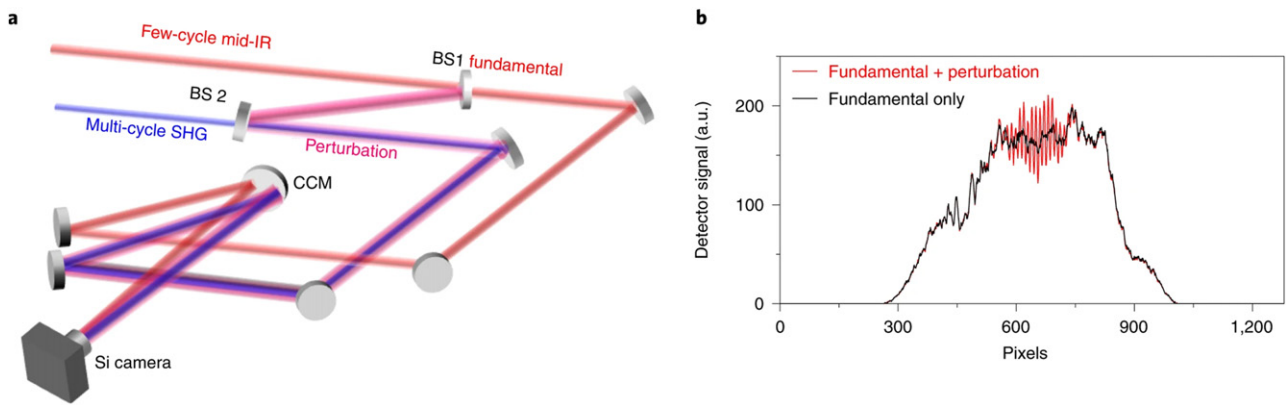
J. Phys. B: At. Mol. Opt. Phys. **55** (2022) 172001

Topical Review

Figure 13. (a) Schematic of the single-shot field-sampler. An intense gate pulse and a weak sample pulse (here, perturbation) are focused with a cylindrical mirror onto a silicon-based image sensor for mapping the temporal delay to a transverse spatial coordinate. The gate pulse drives multiphoton excitation in the silicon chip, while the sample pulse perturbs this process. BS: beamsplitter; CCM: concave cylindrical mirror. (b) The frequency domain representation of the induced perturbation of the weak sample pulse on the intense fundamental pulse [68].
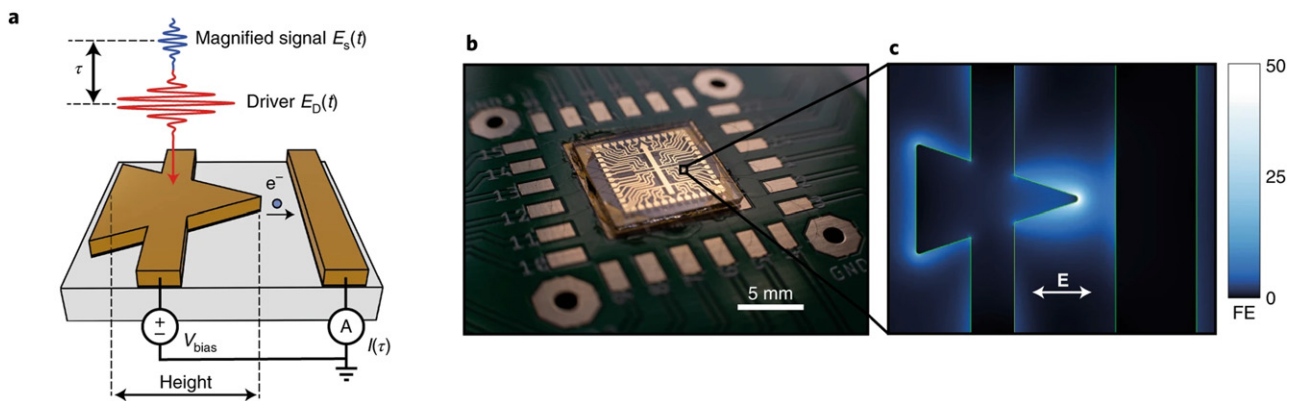

Figure 14. (a) Schematic design of the nanoantennas. A strong driver pulse generates short electron bursts, that can be detected as a current. The weaker sample pulse can be detected as a modulation in this current. (b) Pictures of the nanocircuit embedded on a printed circuit board. (c) Simulated electric field enhancement around a nanoantenna. E indicates the polarization direction of the incident electric field [64].

acousto-optical delay line is limited to one octave with a diffraction efficiency inversely proportional to the spectral bandwidth, making their application for few-cycle pulses limited [131].

4.3. Scanning mechanical resonator

A rapid scanning delay line can be created by employing a reflecting surface such as a glued mirror or a coated gold layer onto the end surface of a mechanical resonator [134–136] (figure 11) [134, 136]. For an incident train of pulses, the sonotrode delay line scans the optical path length from zero to the peak-to-peak amplitude, which is in the order of 100–200 μm, corresponding to a time delay of several hundreds of femtoseconds. Therefore, multiple reflections on the moving surface are required in order to increase the scanning range.

The step size and the duty time of the scan depends on the specific scanning frequency of the delay line and the repetition rate of the laser. Here, the scanning frequency is two times the frequency of the mechanical oscillation, since a scan can be performed in both directions. Typical values for resonant frequencies of such mechanical oscillators lay in the range of sev-

eral tens of kilohertz. Due to its rapid mechanical movement, the sonotrode based delay line is prone to beam pointing fluctuations, where multiple reflections on the oscillating surface increase the influence of slight imperfections of the sonotrode, resulting in even higher fluctuations [136].

4.4. Translating-wedge-based identical pulses encoding system

Since conventional delay lines split a beam into two separate paths with different optical lengths, mechanical vibrations in one arm (e.g. due to a moving delay stage) may not affect the other beam path. Accordingly, such asymmetric mechanical vibrations between the two beam paths can result in fluctuations of the optical length difference. This can lead to additional jitter in the introduced time delay between the pulses. A common path delay line, like the translating-wedge-based identical pulses encoding system (TWINS), can circumvent this problem [137, 138]. TWINS has been used in a number of different applications such as 2D-spectroscopy [138], hyper-spectral imaging [139] or stimulated Raman scattering [140].
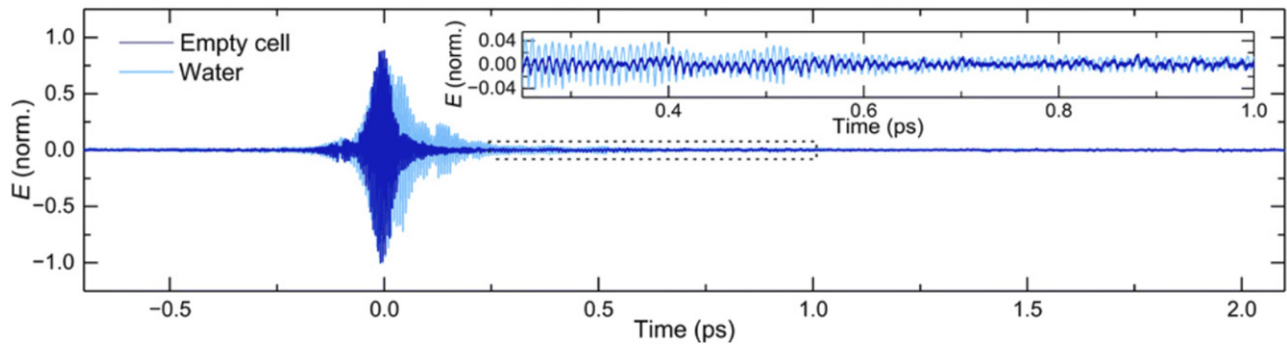
Figure 15. Direct electric field detection of the molecular response of water when excited by laser pulses at 1.9 μm. Reprinted from [24]. (c) The authors, some rights reserved; exclusive licensee AAAS. Distributed under a CC BY-NC 4.0 license http://creativecommons.org/licenses/by-nc/4.0/.

The working principle of TWINS is depicted in figure 12. The system consists of one flat block and two wedge pairs consisting of an uniaxial crystal. The optical axis of the first block A is chosen to be oriented in x-direction. Therefore, an incoming pulse, polarized linearly at 45°, is split evenly to an extraordinary and an ordinary components. Since the two normal modes see different group indices n_e^g and n_o^g, they travel at different group velocities and are temporally separated after the crystal.

The delay between the two pulses after the first block is a constant initial delay. The variability of the optical delay between the pulses is introduced in the second pair of wedges B placed on a translation stage. Here, the optical axis is orientated in z-direction for the first wedge and in y-direction for the second wedge. Therefore, both pulses experience the same ordinary group index for the first wedge. In the second wedge, the optical axis of the crystal is rotated by 90° with respect to block A. Hence, the orientation of the ordinary axis of block A corresponds to the extraordinary axis of the second wedge in wedge pair B. This arrangement allows to counteract the initial introduced time delay between the two pulses since the previous fast (slow) axis becomes the slow (fast) axis. The pulses experience different time delays at different wedge position [138].

Employing TWINS offers attosecond temporal resolution with the temporal jitter limited to ~5 as over 30 min operation [137, 138, 141, 142]. However, since TWINS acknowledgerely on a mechanical moving delay stage, the scan rate of the delay line is limited by the speed of the stage from the sub-Hz to Hz-regime. Furthermore, the tunable temporal delay is limited by the design of the wedges and limited to 1 ps [138, 140, 143].

5. On chip electric field sampling

Until now, we discussed several novel techniques as feasible paths for the direct optical-field acknowledged sampling of an arbitrary waveform at PHz frequencies and in ambient air. While these techniques are used routinely for laboratory-scale measurements, they are seldom accessible for industrial-grade and real-world applications. All these methods require intense, near-single cycle, CEP-stable laser pulses to drive the

fast gate, which requires bulky and expensive amplifiers that are primarily operating at kilohertz repetition rates.

For multi-shot measurements, excellent pulse-to-pulse stability is essential for enhancing the detection sensitivity, which is cumbersome at kilohertz repetition rates. Scaling the repetition rates to megahertz should allow higher laser stability down to the shot-noise limit due to the inverse scaling of the laser noise with its repetition rate. Despite the amazing progress of laser technology in recent years [25, 144–149], generation of CEP-stable pulses at sufficiently high peak-power and average-power remains cumbersome.

Two recent advancements tackle these shortcomings. Liu *et al* [68] report on the first single-shot field sampling at kilohertz repetition rates, while Bionta *et al* [64] demonstrate a sensitive field sampling device suitable for low peak-power, high repetition rate lasers. The two techniques are discussed in the following.

Liu *et al* achieve the single-shot field-sampling of a weak sample pulse in an approach similar to TIPTOE. Here, the temporal delay between the weak sample pulse and an intense pulse are mapped onto a transverse spatial coordinate of a silicon-based image sensor chip [68]. The intense pulses at 3.4 μm create charge packets in the image sensor via multi-photon excitation. At the same time, the co-propagating weak waveform perturbs the probability of the excitation, leading to modulation in the excitation probability and, therefore, the magnitude of the detected photocurrent. In a geometry similar to [150] the time delay is mapped onto a transverse spatial coordinate by crossing the two beams with cylindrical focusing, enabling a single-shot field sampling of the weak pulse (figure 13). The detection bandwidth of such a scheme can be extended to higher frequencies by using different detector technologies, like ZnO [69] or AlGaN [151] sensors.

The on-chip, hyper-sensitive, field sampling technique demonstrated by Bionta *et al* addresses the lack of compact and integratable field-samplers at PHz frequencies [64]. Similar to solids, the photoemission from plasmonic nanoantennas shows a dependence on the CEP of the laser pulses, resulting in a sub-cycle optical-field emission [152–156]. The concept for miniaturizing the optical field-sampling technology is described in figure 14.

The device consists of an array of plasmonic gold nanoantennas, gold nanowires, and an external current detector. The nanoantenna functions as an electron source. Upon the interaction of strong few-cycle laser pulses and the nanoantenna/wire junction, optical-field-controlled electron bursts with the duration of several hundreds of attoseconds are emitted [157–159]. Owing to field enhancement at the tip, 50 pJ pulse energy is adequate to drive the attosecond electron bursts. In the presence of a weak sample pulse, the detected current can be described as:

$$I(\tau) \propto \int_{-T_{\text{rep}}/2}^{T_{\text{rep}}/2} \left(\Gamma(E_{\text{D}}^{\text{L}}(t-\tau)) + \frac{\text{d}\Gamma}{\text{d}E} E_{\text{s}}^{\text{L}}(t) \right) \text{d}t, \qquad (5)$$

where $I(\tau)$ describes the measured current, Γ nonlinear emission rate [160], E_{D}^{L} the local electric field at the nanoantenna tip, E_{s}^{L} weak local signal field, T_{rep} the repetition rate of the laser, and τ the relative delay between the two interacting pulses. The second term in equation (5) is a cross-correlation term and its Fourier transform describes the full sampling response to the weak sample pulse. Therefore, scanning the delay between the two pulses and recording the modulated current allows direct electric-field sampling.

The authors demonstrate six orders of magnitude higher detection sensitivity than the current state of the art in this spectral range. Therefore, a compact and affordable laser oscillator combined with the electric field enhancement from an integratable nanoantenna could solve the complexity of the frontend of the current field samplers. Moreover, the numerical investigation predicts up to 1 PHz detection bandwidth, limited by the work function of the gold device and linear photoemission due to single-photon absorption. Furthermore, the nanoantennas are electrically wired together, and 10–15 of them are irradiated simultaneously and have a contribution to the detected current, making the device amenable to large-scale electronic integration [161, 162].

However, in this scheme, special attention needs to be paid on the intensity of the strong pulse, and the relative intensity of the strong and weak pulses. At high intensities, the nanostructures experience deformation and changes in the resonance of the antenna [163], which eventually results in degradation of the photocurrent and increasing the measurement's noise away from shot-noise [161]. This also adds a limitation on irradiation time and average power scalability of the device.

6. Summary and future perspectives

In this paper we have reviewed the recent techniques for direct electric-field sampling at optical frequencies and in ambient air, overcoming the bandwidth limitations of the traditional field detection schemes. All techniques have a commutual requirement: a short auxiliary event to probe the electric field of light in the time domain. Such short events are generated either (i) from the strong-field interaction of a near-single-cycle laser pulse with matter, or (ii) by temporal compression of an optical gate pulse with a central frequency higher than the central frequency of the pulse to be measured.

In contrast to techniques that characterize solely the complex pulse envelope based on perturbative nonlinear optics, the field measurement techniques do not require reconstruction algorithms and allow for complete characterization of the electric field with a bandwidth approaching 1.5 PHz. Nonetheless, the temporal resolution of field-detectors is prone to the temporal jitter, and they require intense, CEP-stable laser pulse. On-chip field-resolved techniques significantly lower the required intensity of strong-field methods and is keeping promise for integratable field-samplers at PHz frequencies.

These recent advances offer new prospects in studying sub-cycle light–matter interactions such as attosecond electron dynamics and optical-field-driven nonlinear phenomena and is opening up new horizons in spectro-microscopy at extreme limits. PHz field-sampling, based on EOS has been already employed for sensitive field-resolved detection of the response of water molecules when excited at 1.9 μm in ambient air (figure 15) [24, 164].

Besides the high detection dynamic range and sensitivity, the technique offers a great potential for high-resolution, label-free spectro-microscopy. Vibrational microscopy has been a method of choice for the non-perturbative, label-free identification of complex molecular composition and offers intrinsic chemical selectivity due to the specific vibrational frequency of different molecules [140, 165–170]. However, the spatial resolution of the current generation label-free microscopes is limited to Abbe's diffraction limit and unable to access molecular composition in live biological systems at a high spatial resolution. When vibrational microscopy is combined with nonlinear EOS, label-free images with a spatial resolution below the diffraction limit of the excitation pulses could be captured, as here the spatial resolution of the captured image is defined by the diffraction limit of the gate pulses [171]. Recent trends in PHz field-sampling are opening new routes for advancing precision spectroscopy down to sub-cycle regime and opening new eras in field-resolve spectro-microscopy.

Data availability statement

No new data were created or analysed in this study.

ORCID iDs

A Herbst ⓘ https://orcid.org/0000-0002-2415-0260
M M Bidhendi ⓘ https://orcid.org/0000-0002-9283-1105
A Srivastava ⓘ https://orcid.org/0000-0003-2883-3007
H Fattahi ⓘ https://orcid.org/0000-0002-6485-529X

J. Phys. B: At. Mol. Opt. Phys. **55** (2022) 172001

Topical Review

References

[1] Zewail A H 2000 Femtochemistry: atomic-scale dynamics of the chemical bond *J. Phys. Chem.* A **104** 5660–94

[2] Shank C V and Ippen E P 1974 Subpicosecond kilowatt pulses from a mode-locked cw dye laser *Appl. Phys. Lett.* **24** 373–5

[3] Baltuška A, Wei Z, Pshenichnikov M S and Wiersma D A 1997 Optical pulse compression to 5 fs at a 1-MHz repetition rate *Opt. Lett.* **22** 102–4

[4] Zhou J, Christov I P, Taft G, Huang C-P, Murnane M M and Kapteyn H C 1994 Pulse evolution in a broad-bandwidth Ti:sapphire laser *Opt. Lett.* **19** 1149–51

[5] Spence D E, Kean P N and Sibbett W 1991 60-fsec pulse generation from a self-mode-locked Ti:sapphire laser *Opt. Lett.* **16** 42–4

[6] Fork R L, Brito Cruz C H, Becker P C and Shank C V 1987 Compression of optical pulses to six femtoseconds by using cubic phase compensation *Opt. Lett.* **12** 483–5

[7] Alfano R R and Shapiro S L 1970 Emission in the region 4000 to 7000 Å via four-photon coupling in glass *Phys. Rev. Lett.* **24** 584–7

[8] Holzwarth R, Udem T, Hänsch T W, Knight J C, Wadsworth W J and Russell P S J 2000 Optical frequency synthesizer for precision spectroscopy *Phys. Rev. Lett.* **85** 2264–7

[9] Udem T, Holzwarth R and Hänsch T W 2002 Optical frequency metrology *Nature* **416** 233–7

[10] Baltuška A *et al* 2003 Attosecond control of electronic processes by intense light fields *Nature* **421** 611–5

[11] Hänsch T W 2006 Nobel lecture: passion for precision *Rev. Mod. Phys.* **78** 1297–309

[12] Hall J L 2006 Nobel lecture: defining and measuring optical frequencies *Rev. Mod. Phys.* **78** 1279–95

[13] Telle H R, Steinmeyer G, Dunlop A E, Stenger J, Sutter D H and Keller U 1999 Carrier-envelope offset phase control: a novel concept for absolute optical frequency measurement and ultrashort pulse generation *Appl. Phys.* B **69** 327–32

[14] Krausz F and Ivanov M 2009 Attosecond physics *Rev. Mod. Phys.* **81** 163–234

[15] Szipöcs R, Spielmann C, Krausz F and Ferencz K 1994 Chirped multilayer coatings for broadband dispersion control in femtosecond lasers *Opt. Lett.* **19** 201–3

[16] Kärtner F X, Morgner U, Ell R, Schibli T, Fujimoto J G, Ippen E P, Scheuer V, Angelow G and Tschudi T 2001 Ultrabroadband double-chirped mirror pairs for generation of octave spectra *J. Opt. Soc. Am.* B **18** 882–5

[17] Pervak V, Ahmad I, Trubetskov M K, Tikhonravov A V and Krausz F 2009 Double-angle multilayer mirrors with smooth dispersion characteristics *Opt. Express* **17** 7943–51

[18] Tournois P 1997 Acousto-optic programmable dispersive filter for adaptive compensation of group delay time dispersion in laser systems *Opt. Commun.* **140** 245–9

[19] Weiner A M 2000 Femtosecond pulse shaping using spatial light modulators *Rev. Sci. Instrum.* **71** 1929–60

[20] Weiner A M 2011 Ultrafast optical pulse shaping: a tutorial review *Opt. Commun.* **284** 3669–92

[21] Wirth A *et al* 2011 Synthesized light transients *Science* **334** 195–200

[22] Hassan M T *et al* 2016 Optical attosecond pulses and tracking the nonlinear response of bound electrons *Nature* **530** 66–70

[23] Manzoni C, Huang S W, Cirmi G, Moses J, Kärtner F X and Cerullo G 2012 Coherent synthesis of ultra-broadband optical parametric amplifiers *Research in Optical Sciences* p HT3C.5

[24] Alismail A *et al* 2020 Multi-octave, CEP-stable source for high-energy field synthesis *Sci. Adv.* **6** eaax3408

[25] Fattahi H *et al* 2014 Third-generation femtosecond technology *Optica* **1** 45–63

[26] Hassan M T, Wirth A, Grguraš I, Moulet A, Luu T T, Gagnon J, Pervak V and Goulielmakis E 2012 Invited article: attosecond photonics: synthesis and control of light transients *Rev. Sci. Instrum.* **83** 111301

[27] Rossi G M *et al* 2020 Sub-cycle millijoule-level parametric waveform synthesizer for attosecond science *Nat. Photon.* **14** 629–35

[28] Hui D, Alqattan H, Zhang S, Pervak V, Chowdhury E and Hassan M 2022 Nature portfolio available from: ⟨https://doi.org/10.21203/rs.3.rs-1232650/v1⟩

[29] Mauritsson J *et al* 2010 Attosecond electron spectroscopy using a novel interferometric pump-probe technique *Phys. Rev. Lett.* **105** 053001

[30] Kling M F *et al* 2006 Control of electron localization in molecular dissociation *Science* **312** 246–8

[31] Sansone G *et al* 2006 Isolated single-cycle attosecond pulses *Science* **314** 443–6

[32] Cavalieri A L *et al* 2007 Attosecond spectroscopy in condensed matter *Nature* **449** 1029–32

[33] Trebino R 2000 *Frequency-Resolved Optical Gating: The Measurement of Ultrashort Laser Pulses* (New York: Springer Science+Business Media, LLC) ⟨https://doi.org/10.1007/978-1-4615-1181-6⟩

[34] Kane D J and Trebino R 1993 Characterization of arbitrary femtosecond pulses using frequency-resolved optical gating *IEEE J. Quantum Electron.* **29** 571–9

[35] Nomura Y, Shirai H and Fuji T 2013 Frequency-resolved optical gating capable of carrier-envelope phase determination *Nat. Commun.* **4** 2820

[36] Iaconis C and Walmsley I A 1998 Spectral phase interferometry for direct electric-field reconstruction of ultrashort optical pulses *Opt. Lett.* **23** 792–4

[37] Miranda M, Arnold C L, Fordell T, Silva F, Alonso B, Weigand R, L'Huillier A and Crespo H 2012 Characterization of broadband few-cycle laser pulses with the d-scan technique *Opt. Express* **20** 18732–43

[38] Tsang T, Krumbügel M A, DeLong K W, Fittinghoff D N and Trebino R 1996 Frequency-resolved optical-gating measurements of ultrashort pulses using surface third-harmonic generation *Opt. Lett.* **21** 1381–3

[39] Kane D J and Trebino R 1993 Single-shot measurement of the intensity and phase of an arbitrary ultrashort pulse by using frequency-resolved optical gating *Opt. Lett.* **18** 823–5

[40] DeLong K W, Trebino R, Hunter J and White W E 1994 Frequency-resolved optical gating with the use of second-harmonic generation *J. Opt. Soc. Am.* B **11** 2206–15

[41] Linden S, Kuhl J and Giessen H 1999 Amplitude and phase characterization of weak blue ultrashort pulses by downconversion *Opt. Lett.* **24** 569–71

[42] Sweetser J N, Fittinghoff D N and Trebino R 1997 Transient-grating frequency-resolved optical gating *Opt. Lett.* **22** 519–21

[43] Jones T, Peters W K, Efimov A, Sandberg R L, Yarotski D, Trebino R and Bowlan P 2020 Encoding the complete electric field of an ultraviolet ultrashort laser pulse in a near-infrared nonlinear-optical signal *Opt. Express* **28** 26850–60

[44] Gallmann L, Sutter D H, Matuschek N, Steinmeyer G, Keller U, Iaconis C and Walmsley I A 1999 Characterization of sub-6-fs optical pulses with spectral phase interferometry for direct electric-field reconstruction *Opt. Lett.* **24** 1314–6

[45] Stibenz G and Steinmeyer G 2004 High dynamic range characterization of ultrabroadband white-light continuum pulses *Opt. Express* **12** 6319–25

[46] Dorrer C, Londero P and Walmsley I A 2001 Homodyne detection in spectral phase interferometry for direct electric-field reconstruction *Opt. Lett.* **26** 1510–2

J. Phys. B: At. Mol. Opt. Phys. **55** (2022) 172001

Topical Review

[47] Hirasawa M, Nakagawa N, Yamamoto K, Morita R, Shigekawa H and Yamashita M 2002 Sensitivity improvement of spectral phase interferometry for direct electric-field reconstruction for the characterization of low-intensity femtosecond pulses *Appl. Phys.* B **74** 225–9

[48] Londero P, Anderson M E, Radzewicz C, Iaconis C and Walmsley I A 2003 Measuring ultrafast pulses in the near-ultraviolet using spectral phase interferometry for direct electric field reconstruction *J. Mod. Opt.* **50** 179–84

[49] Dorrer C and Kang I 2003 Highly sensitive direct characterization of femtosecond pulses by electro-optic spectral shearing interferometry *Opt. Lett.* **28** 477–9

[50] Baum P and Riedle E 2005 Design and calibration of zero-additional-phase SPIDER *J. Opt. Soc. Am.* B **22** 1875–83

[51] Wyatt A S, Walmsley I A, Stibenz G and Steinmeyer G 2006 Sub-10 fs pulse characterization using spatially encoded arrangement for spectral phase interferometry for direct electric field reconstruction *Opt. Lett.* **31** 1914–6

[52] Birge J R, Ell R and Kärtner F X 2006 Two-dimensional spectral shearing interferometry for few-cycle pulse characterization *Opt. Lett.* **31** 2063–5

[53] Pasquazi A, Peccianti M, Park Y, Little B E, Chu S T, Morandotti R, Azaña J and Moss D J 2011 Sub-picosecond phase-sensitive optical pulse characterization on a chip *Nat. Photon.* **5** 618–23

[54] Lei C, Guo B, Cheng Z and Goda K 2016 Optical time-stretch imaging: principles and applications *Appl. Phys. Rev.* **3** 011102

[55] Cousin S L, Bueno J M, Forget N, Austin D R and Biegert J 2012 Three-dimensional spatiotemporal pulse characterization with an acousto-optic pulse shaper and a Hartmann–Shack wavefront sensor *Opt. Lett.* **37** 3291–3

[56] Fittinghoff D N, Walmsley I A, Bowie J L, Sweetser J N, Jennings R T, Krumbügel M A, DeLong K W and Trebino R 1996 Measurement of the intensity and phase of ultraweak, ultrashort laser pulses *Opt. Lett.* **21** 884–6

[57] Alonso B, Sola Í J and Crespo H 2018 Self-calibrating d-scan: measuring ultrashort laser pulses on-target using an arbitrary pulse compressor *Sci. Rep.* **8** 1–8

[58] Leblanc A *et al* 2019 Phase-matching-free pulse retrieval based on transient absorption in solids *Opt. Express* **27** 28998–9015

[59] Zimin D A, Yakovlev V S and Karpowicz N 2021 Ultra-broadband photonic sampling of optical waveforms (arXiv: 2111.09864)

[60] Alonso B, Miranda M, Sola Í J and Crespo H 2012 Spatiotemporal characterization of few-cycle laser pulses *Opt. Express* **20** 17880–93

[61] Silva F, Miranda M, Alonso B, Rauschenberger J, Pervak V and Crespo H 2014 Simultaneous compression, characterization and phase stabilization of GW-level 14 cycle VIS-NIR femtosecond pulses using a single dispersion-scan setup *Opt. Express* **22** 10181–91

[62] Kurucz M, Tóth S, Flender R, Haizer L, Kiss B, Persielle B and Cormier E 2019 Single-shot CEP drift measurement at arbitrary repetition rate based on dispersive Fourier transform *Opt. Express* **27** 13387–99

[63] Sederberg S *et al* 2020 Attosecond optoelectronic field measurement in solids *Nat. Commun.* **11** 430

[64] Bionta M R, Ritzkowsky F, Turchetti M, Yang Y, Cattozzo Mor D, Putnam W P, Kärtner F X, Berggren K K and Keathley P D 2021 On-chip sampling of optical fields with attosecond resolution *Nat. Photon.* **15** 456–60

[65] Zimin D, Weidman M, Schötz J, Kling M F, Yakovlev V S, Krausz F and Karpowicz N 2021 Petahertz-scale nonlinear photoconductive sampling in air *Optica* **8** 586–90

[66] Hui D, Alqattan H, Yamada S, Pervak V, Yabana K and Hassan M T 2022 Attosecond electron motion control in dielectric *Nat. Photon.* **16** 33–7

[67] Cho W, Hwang S I, Nam C H, Bionta M R, Lassonde P, Schmidt B E, Ibrahim H, Légaré F and Kim K T 2019 Temporal characterization of femtosecond laser pulses using tunneling ionization in the UV, visible, and mid-IR ranges *Sci. Rep.* **9** 16067

[68] Liu Y, Beetar J E, Nesper J, Gholam-Mirzaei S and Chini M 2021 Single-shot measurement of few-cycle optical waveforms on a chip *Nat. Photon.* **16** 109

[69] Liu Y, Gholam-Mirzaei S, Beetar J E, Nesper J, Yousif A, Nrisimhamurty M and Chini M 2021 All-optical sampling of few-cycle infrared pulses using tunneling in a solid *Photon. Res.* **9** 929–36

[70] Pupeza I *et al* 2020 Field-resolved infrared spectroscopy of biological systems *Nature* **577** 52–9

[71] Korobenko A *et al* 2020 Femtosecond streaking in ambient air *Optica* **7** 1372–6

[72] Kowligy A S, Timmers H, Lind A J, Elu U, Cruz F C, Schunemann P G, Biegert J and Diddams S A 2019 Infrared electric field sampled frequency comb spectroscopy *Sci. Adv.* **5** eaaw8794

[73] Wu Q and Zhang X C 1996 Ultrafast electro-optic field sensors *Appl. Phys. Lett.* **68** 1604–6

[74] Szwaj C, Evain C, Le Parquier M, Roy P, Manceron L, Brubach J-B, Tordeux M-A and Bielawski S 2016 High sensitivity photonic time-stretch electro-optic sampling of terahertz pulses *Rev. Sci. Instrum.* **87** 103111

[75] Auston D H, Johnson A M, Smith P R and Bean J C 1980 Picosecond optoelectronic detection, sampling, and correlation measurements in amorphous semiconductors *Appl. Phys. Lett.* **37** 371–3

[76] Riek C, Seletskiy D V, Moskalenko A S, Schmidt J F, Krauspe P, Eckart S, Eggert S, Burkard G and Leitenstorfer A 2015 Direct sampling of electric-field vacuum fluctuations *Science* **350** 420–3

[77] Benea-Chelmus I C, Settembrini F F, Scalari G and Faist J 2019 Electric field correlation measurements on the electromagnetic vacuum state *Nature* **568** 202–6

[78] Guedes T L M, Kizmann M, Seletskiy D V, Leitenstorfer A, Burkard G and Moskalenko A S 2019 Spectra of ultrabroadband squeezed pulses and the finite-time Unruh–Davies effect *Phys. Rev. Lett.* **122** 053604

[79] Riek C, Sulzer P, Seeger M, Moskalenko A S, Burkard G, Seletskiy D V and Leitenstorfer A 2017 Subcycle quantum electrodynamics *Nature* **541** 376–9

[80] Riek C, Seletskiy D V and Leitenstorfer A 2017 Femtosecond measurements of electric fields: from classical amplitudes to quantum fluctuations *Eur. J. Phys.* **38** 024003

[81] Bonvalet A, Nagle J, Berger V, Migus A, Martin J L and Joffre M 1996 Femtosecond infrared emission resulting from coherent charge oscillations in quantum wells *Phys. Rev. Lett.* **76** 4392–5

[82] Schubert O *et al* 2014 Sub-cycle control of terahertz high-harmonic generation by dynamical Bloch oscillations *Nat. Photon.* **8** 119–23

[83] Hohenleutner M, Langer F, Schubert O, Knorr M, Huttner U, Koch S W, Kira M and Huber R 2015 Real-time observation of interfering crystal electrons in high-harmonic generation *Nature* **523** 572–5

[84] Grischkowsky D, Keiding S, van Exter M and Fattinger C 1990 2015 Far-infrared time-domain spectroscopy with terahertz beams of dielectrics and semiconductors *J. Opt. Soc. Am.* B **7** 2006

[85] Fischer M P *et al* 2021 Field-resolved detection of the temporal response of a single plasmonic antenna in the mid-infrared *Optica* **8** 898–903

J. Phys. B: At. Mol. Opt. Phys. **55** (2022) 172001

Topical Review

[86] Hentschel M *et al* 2001 Attosecond metrology *Nature* **414** 509–13

[87] Goulielmakis E *et al* 2004 Direct measurement of light waves *Science* **305** 1267–9

[88] Itatani J, Quéré F, Yudin G L, Ivanov M Y, Krausz F and Corkum P B 2002 Attosecond streak camera *Phys. Rev. Lett.* **88** 173903

[89] Kienberger R *et al* 2004 Atomic transient recorder *Nature* **427** 817–21

[90] Kim K T *et al* 2013 Petahertz optical oscilloscope *Nat. Photon.* **7** 958–62

[91] Wyatt A S *et al* 2016 Attosecond sampling of arbitrary optical waveforms *Optica* **3** 303–10

[92] Chini M, Zhao K and Chang Z 2014 The generation, characterization and applications of broadband isolated attosecond pulses *Nat. Photon.* **8** 178–86

[93] Reiss H R 1980 Effect of an intense electromagnetic field on a weakly bound system *Phys. Rev.* A **22** 1786–813

[94] Keldysh L V 1965 Ionization in the field of a strong electromagnetic wave *Sov. Phys. JETP* **20** 1307–14

[95] Khurgin J B 2016 Optically induced currents in dielectrics and semiconductors as a nonlinear optical effect *J. Opt. Soc. Am.* B **33** C1–9

[96] Paasch-Colberg T *et al* 2016 Sub-cycle optical control of current in a semiconductor: from the multiphoton to the tunneling regime *Optica* **3** 1358–61

[97] Schultze M *et al* 2013 Controlling dielectrics with the electric field of light *Nature* **493** 75–8

[98] Schiffrin A *et al* 2013 Optical-field-induced current in dielectrics *Nature* **493** 70–4

[99] Apalkov V and Stockman M I 2012 Theory of dielectric nanofilms in strong ultrafast optical fields *Phys. Rev.* B **86** 165118

[100] Kruchinin S Y, Krausz F and Yakovlev V S 2018 Colloquium: strong-field phenomena in periodic systems *Rev. Mod. Phys.* **90** 021002

[101] Wachter G, Lemell C, Burgdörfer J, Sato S A, Tong X M and Yabana K 2014 *Ab Initio* simulation of electrical currents induced by ultrafast laser excitation of dielectric materials *Phys. Rev. Lett.* **113** 087401

[102] Colosimo P *et al* 2008 Scaling strong-field interactions towards the classical limit *Nat. Phys.* **4** 386–9

[103] DiMauro L, Frolov M, Ishikawa K L and Ivanov M 2014 50 years of optical tunneling *J. Phys. B: At. Mol. Opt. Phys.* **47** 200301

[104] Park S B, Kim K, Cho W, Hwang S I, Ivanov I, Nam C H and Kim K T 2018 Direct sampling of a light wave in air *Optica* **5** 402–8

[105] Saito N, Ishii N, Kanai T and Itatani J 2018 All-optical characterization of the two-dimensional waveform and the Gouy phase of an infrared pulse based on plasma fluorescence of gas *Opt. Express* **26** 24591–601

[106] Ivanov M and Smirnova O 2011 How accurate is the attosecond streak camera? *Phys. Rev. Lett.* **107** 213605

[107] Landsman A S and Keller U 2015 Attosecond science and the tunnelling time problem *Phys. Rep.* **547** 1–24

[108] Pazourek R, Nagele S and Burgdörfer J 2015 Attosecond chronoscopy of photoemission *Rev. Mod. Phys.* **87** 765–802

[109] Ghimire S and Reis D A 2019 High-harmonic generation from solids *Nat. Phys.* **15** 10–6

[110] Fonoberov V A, Alim K A, Balandin A A, Xiu F and Liu J 2006 Photoluminescence investigation of the carrier recombination processes in ZnO quantum dots and nanocrystals *Phys. Rev.* B **73** 165317

[111] Rodnyi P A and Khodyuk I V 2011 Optical and luminescence properties of zinc oxide (review) *Opt. Spectrosc.* **111** 776–85

[112] Nahata A, Weling A S and Heinz T F 1996 A wideband coherent terahertz spectroscopy system using optical rectification and electro-optic sampling *Appl. Phys. Lett.* **69** 2321–3

[113] Leitenstorfer A, Hunsche S, Shah J, Nuss M C and Knox W H 1999 Detectors and sources for ultrabroadband electro-optic sampling: experiment and theory *Appl. Phys. Lett.* **74** 1516–8

[114] Kübler C, Huber R, Tübel S and Leitenstorfer A 2004 Ultrabroadband detection of multi-terahertz field transients with GaSe electro-optic sensors: approaching the near infrared *Appl. Phys. Lett.* **85** 3360–2

[115] Sell A, Scheu R, Leitenstorfer A and Huber R 2008 Field-resolved detection of phase-locked infrared transients from a compact Er:fiber system tunable between 55 and 107 THz *Appl. Phys. Lett.* **93** 251107

[116] Keiber S, Sederberg S, Schwarz A, Trubetskov M, Pervak V, Krausz F and Karpowicz N 2016 Electro-optic sampling of near-infrared waveforms *Nat. Photon.* **10** 159–62

[117] Wang H, Alismail A, Barbiero G, Ahmad R N and Fattahi H 2019 High energy, sub-cycle, field synthesizers *IEEE J. Sel. Top. Quantum Electron.* **25** 1–12

[118] Gallot G and Grischkowsky D 1999 Electro-optic detection of terahertz radiation *J. Opt. Soc. Am.* B **16** 1204–12

[119] Sulzer P *et al* 2020 Determination of the electric field and its Hilbert transform in femtosecond electro-optic sampling *Phys. Rev.* A **101** 033821

[120] Bidhendi M M 2021 *Controlling Temporal Jitter in Direct Electric-Field Sampling* (Friedrich Alexander University)

[121] Beckh C, Sulzer P, Fritzsche N, Riek C and Leitenstorfer A 2021 Analysis of subcycle electro-optic sampling without background *J. Infrared Millim. Terahertz Waves* **42** 701–14

[122] Porer M, Ménard J M and Huber R 2014 Shot noise reduced terahertz detection via spectrally postfiltered electro-optic sampling *Opt. Lett.* **39** 2435–8

[123] Boyd R W 2008 *Nonlinear Optics* 3rd edn (Oxford: Elsevier Inc.)

[124] Dai J, Xie X and Zhang X C 2006 Detection of broadband terahertz waves with a laser-induced plasma in gases *Phys. Rev. Lett.* **97** 103903

[125] Karpowicz N *et al* 2008 Coherent heterodyne time-domain spectrometry covering the entire 'terahertz gap' *Appl. Phys. Lett.* **92** 011131

[126] Feldstein M J, Vöhringer P and Scherer N F 1995 Rapid-scan pump–probe spectroscopy with high time and wave-number resolution: optical-Kerr-effect measurements of neat liquids *J. Opt. Soc. Am.* B **12** 1500–10

[127] Withayachumnankul W, Lin H, Mickan S P, Fischer B M and Abbott D 2007 Analysis of measurement uncertainty in THz-TDS *Photonic Materials, Devices, and Applications II* vol 6593 ed A Serpengüzel, G Badenes and G C Righini (Bellingham, WA: SPIE Optical Engineering Press) pp 604–21

[128] Schweinberger W, Vamos L, Xu J, Hussain S A, Baune C, Rode S and Pupeza I 2019 Interferometric delay tracking for low-noise Mach–Zehnder-type scanning measurements *Opt. Express* **27** 4789–98

[129] Schubert O, Eisele M, Crozatier V, Forget N, Kaplan D and Huber R 2013 Rapid-scan acousto-optical delay line with 34 kHz scan rate and 15 as precision *Opt. Lett.* **38** 2907–10

[130] Znakovskaya I, Fill E, Forget N, Tournois P, Seidel M, Pronin O, Krausz F and Apolonski A 2014 Dual frequency comb spectroscopy with a single laser *Opt. Lett.* **39** 5471–4

[131] Urbanek B, Möller M, Eisele M, Baierl S, Kaplan D, Lange C and Huber R 2016 Femtosecond terahertz time-domain spectroscopy at 36 kHz scan rate using an acousto-optic delay *Appl. Phys. Lett.* **108** 121101

[132] Audier X, Balla N and Rigneault H 2017 Pump-probe microspectroscopy by means of an ultra-fast acousto-optics delay line *Opt. Lett.* **42** 294–7

J. Phys. B: At. Mol. Opt. Phys. 55 (2022) 172001

Topical Review

[133] Alshaykh M S, Liao C S, Sandoval O E, Gitzinger G, Forget N, Leaird D E, Cheng J-X and Weiner A M 2017 High-speed stimulated hyperspectral Raman imaging using rapid acousto-optic delay lines *Opt. Lett.* **42** 1548–51

[134] Süss B, Ringleb F and Heberle J 2016 New ultrarapid-scanning interferometer for FT-IR spectroscopy with microsecond time-resolution *Rev. Sci. Instrum.* **87** 063113

[135] Jacob P, Weigel A, Gröters D, Buberl T, Trubetskov M, Huber M, Heberle J and Pupeza I 2020 Mid-infrared waveform measurement by rapid mechanical scanning *EPJ Web Conf.* **243** 16002

[136] Buberl T 2021 Towards next-generation molecular finger-printing: advancing mid-infrared spectroscopy for biomedical applications *Dissertation* LMU München: Fakultät für Physik (https://doi.org/10.5282/edoc.27677)

[137] Brida D, Manzoni C and Cerullo G 2012 Phase-locked pulses for two-dimensional spectroscopy by a birefringent delay line *Opt. Lett.* **37** 3027–9

[138] Réhault J, Maiuri M, Oriana A and Cerullo G 2014 Two-dimensional electronic spectroscopy with birefringent wedges *Rev. Sci. Instrum.* **85** 123107

[139] Perri A *et al* 2019 Hyperspectral imaging with a TWINS birefringent interferometer *Opt. Express* **27** 15956–67

[140] Réhault J, Crisafi F, Kumar V, Ciardi G, Marangoni M, Cerullo G and Polli D 2015 Broadband stimulated Raman scattering with Fourier-transform detection *Opt. Express* **23** 25235–46

[141] Réhault J, Maiuri M, Manzoni C, Brida D, Helbing J and Cerullo G 2014 2D IR spectroscopy with phase-locked pulse pairs from a birefringent delay line *Opt. Express* **22** 9063–72

[142] Agathangelou D, El-Khoury Y and Brazard J, Crégut O, Haacke S, Cerullo G and Léonard J 2019 Towards broadband two-Dimensional electronic spectroscopy with 8 fs phase-locked pulses at 400 nm *EPJ Web Conf.* **205** 03006

[143] Oriana A, Réhault J, Preda F, Polli D and Cerullo G 2016 Scanning Fourier transform spectrometer in the visible range based on birefringent wedges *J. Opt. Soc. Am.* A **33** 1415–20

[144] Saraceno C J, Sutter D, Metzger T and Abdou Ahmed M 2019 The amazing progress of high-power ultrafast thin-disk lasers *J. Eur. Opt. Soc.-Rapid Publ.* **15** 15

[145] Zhang J, Schulze F, Mak K F, Pervak V, Bauer D, Sutter D and Pronin O 2018 High-power, high-efficiency Tm:YAG and Ho:YAG thin-disk lasers *Laser Photon. Rev.* **12** 1700273

[146] Rudy C W, Digonnet M J F and Byer R L 2014 Advances in 2-μm Tm-doped mode-locked fiber lasers *Opt. Fiber Technol.* **20** 642–9

[147] Ma J, Qin Z, Xie G, Qian L and Tang D 2019 Review of mid-infrared mode-locked laser sources in the 2.0 μm–3.5 μm spectral region *Appl. Phys. Rev.* **6** 021317

[148] Ebrahim-Zadeh M 2008 Mid-infrared optical parametric oscillators and applications *Mid-Infrared Coherent Sources and Applications* ed M Ebrahim-Zadeh and I T Sorokina (Dordrecht: Springer) pp 347–75

[149] Reid D T, Sun J, Lamour T P and Ferreiro T I 2010 Advances in ultrafast optical parametric oscillators *Laser Phys. Lett.* **8** 8–15

[150] Omenetto F G, Nicholson J W and Taylor A J 1999 Single-shot SHG-FROG of ultrashort pulses at 1.55 microns in a compact folded shaper *Ultrafast Electronics and Optoelectronics* p UWC3

[151] Long J P, Varadaraajan J, Matthews J and Schetzina J F 2002 UV detectors and focal plane array imagers based on AlGaN p–i–n photodiodes *Opto-Electron. Rev.* **10** 251–60

[152] Dombi P *et al* 2020 Strong-field nano-optics *Rev. Mod. Phys.* **92** 025003

[153] Krüger M, Lemell C, Wachter G, Burgdörfer J and Hommelhoff P 2018 Attosecond physics phenomena at nanometric tips *J. Phys. B: At. Mol. Opt. Phys.* **51** 172001

[154] Schoetz J, Wang Z, Pisanty E, Lewenstein M, Kling M F and Ciappina M F 2019 Perspective on petahertz electronics and attosecond nanoscopy *ACS Photon.* **6** 3057–69

[155] Ciappina M F *et al* 2017 Attosecond physics at the nanoscale *Rep. Prog. Phys.* **80** 054401

[156] Stockman M I *et al* 2018 Roadmap on plasmonics *J. Opt.* **20** 043001

[157] Ludwig M *et al* 2020 Sub-femtosecond electron transport in a nanoscale gap *Nat. Phys.* **16** 341–5

[158] Keathley P D, Putnam W P, Vasireddy P, Hobbs R G, Yang Y, Berggren K K and Kärtner F X 2019 Vanishing carrier-envelope-phase-sensitive response in optical-field photoemission from plasmonic nanoantennas *Nat. Phys.* **15** 1128–33

[159] Krüger M, Schenk M and Hommelhoff P 2011 Attosecond control of electrons emitted from a nanoscale metal tip *Nature* **475** 78–81

[160] Fowler R H and Nordheim L 1928 Electron emission in intense electric fields *Proc. R. Soc.* A **119** 173–81

[161] Yang Y, Turchetti M, Vasireddy P, Putnam W P, Karnbach O, Nardi A, Kärtner F X, Berggren K K and Keathley P D 2020 Light phase detection with on-chip petahertz electronic networks *Nat. Commun.* **11** 3407

[162] Ludwig M, Kazansky A K, Aguirregabiria G, Marinica D C, Falk M, Leitenstorfer A, Brida D, Aizpurua J and Borisov A G 2020 Active control of ultrafast electron dynamics in plasmonic gaps using an applied bias *Phys. Rev.* B **101** 241412

[163] Putnam W P, Hobbs R G, Keathley P D, Berggren K K and Kärtner F X 2017 Optical-field-controlled photoemission from plasmonic nanoparticles *Nat. Phys.* **13** 335–9

[164] Alismail A *et al* 2019 Near-infrared molecular fieldoscopy of water *Multiphoton Microscopy in the Biomedical Sciences XIX* vol 10882 ed A Periasamy, P T C So and , K König (Bellingham, WA: SPIE Optical Engineering Press) pp 310–5

[165] Evans C L and Xie X S 2008 Coherent anti-Stokes Raman scattering microscopy: chemical imaging for biology and medicine *Annu. Rev. Anal. Chem.* **1** 883–909

[166] Polli D, Kumar V, Valensise C M, Marangoni M and Cerullo G 2018 Broadband coherent Raman scattering microscopy *Laser Photon. Rev.* **12** 1800020

[167] Zhang D, Wang P, Slipchenko M N and Cheng J X 2014 Fast vibrational imaging of single cells and tissues by stimulated Raman scattering microscopy *Acc. Chem. Res.* **47** 2282–90

[168] Pavlovetc I M, Aleshire K, Hartland G V and Kuno M 2020 Approaches to mid-infrared, super-resolution imaging and spectroscopy *Phys. Chem. Chem. Phys.* **22** 4313–25

[169] Mohler K J, Bohn B J, Yan M, Mélen G, Hänsch T W and Picqué N 2017 Dual-comb coherent Raman spectroscopy with lasers of 1-GHz pulse repetition frequency *Opt. Lett.* **42** 318–21

[170] Ideguchi T, Holzner S, Bernhardt B, Guelachvili G, Picqué N and Hänsch T W 2013 Coherent Raman spectro-imaging with laser frequency combs *Nature* **502** 355–8

[171] Fattahi H 2020 *Method and Apparatus for Creating a Microscopic Sample Image of a Molecular Vibrational Response of a Sample* PCT/EP2020/075849